LETTERS
PUBLISHED ONLINE: 31 OCTOBER 2010 | DOI: 10.1038/NPHYS1806
nature physics

Multiple-length-scale elastic instability mimics parametric resonance of nonlinear oscillators

Fabian Brau[1], Hugues Vandeparre[1], Abbas Sabbah[1], Christophe Poulard[1], Arezki Boudaoud[2] and Pascal Damman[1]*

Spatially confined rigid membranes reorganize their morphology in response to the imposed constraints. A crumpled elastic sheet presents a complex pattern of random folds focusing the deformation energy[1], whereas compressing a membrane resting on a soft foundation creates a regular pattern of sinusoidal wrinkles with a broad distribution of energy[2–8]. Here, we study the energy distribution for highly confined membranes and show the emergence of a new morphological instability triggered by a period-doubling bifurcation. A periodic self-organized focalization of the deformation energy is observed provided that an up–down symmetry breaking, induced by the intrinsic nonlinearity of the elasticity equations, occurs. The physical model, exhibiting an analogy with parametric resonance in a nonlinear oscillator, is a new theoretical toolkit to understand the morphology of various confined systems, such as coated materials or living tissues, for example wrinkled skin[3], internal structure of lungs[9], internal elastica of an artery[10], brain convolutions[11,12] or formation of fingerprints[13]. Moreover, it opens the way to a new kind of microfabrication design of multiperiodic or chaotic (aperiodic) surface topography through self-organization.

Several theoretical approaches have been proposed to describe the wrinkling instability for very small compression ratio, that is, near the instability threshold[2,3,7]. However, the large-compression domain remains largely unexplored, with the notable exception of the wrinkle-to-fold transition observed in ref. 8 for an elastic membrane on liquid and the self-similar wrinkling patterns in skins[14]. In the former case, the deformation of the membrane is progressively focalized into a single fold, concentrating all the bending energy. In contrast, for thin rigid membranes on elastomers, large compression induces perturbations of the initial wrinkles but the elasticity of the soft foundation maintains a regular periodic pattern whose complexity increases with the compression ratio.

A polydimethylsiloxane (PDMS) film, stretched and then cured with ultraviolet radiation–ozone, or a thin polymer film bound to an elastomer foundation, remains initially flat. Under a slight compression, $\delta = (L_0 - L)/L_0$, these systems instantaneously form regular (sinusoidal) wrinkles with a well-defined wavelength, λ_0. Increasing δ generates a continuous increase of the amplitude of the wrinkles and a continuous shift to lower wavelength ($\lambda = \lambda_0(1 - \delta)$; see Fig. 1g). By further compression of the sheet, more complex patterns emerge. Above some threshold, $\delta > \delta_2 \simeq 0.2$, we observe a dramatic change in the morphology leading to a pitchfork bifurcation: one wrinkle grows in amplitude at the expense of its neighbours (Fig. 1). The profile of the membrane is no longer described by a single cosinusoid but requires a combination of two periodic functions, $\cos(2\pi x/\lambda)$ and $\cos(2\pi x/2\lambda)$. The amplitude of the 2λ mode increases with the compression ratio, whereas the λ mode vanishes. This effect is similar to period-doubling bifurcations in dynamical systems[15,16] observed in Rayleigh–Bernard convections[17], dynamics of the heart tissue[18–20], oscillated granular matter[21,22] or bouncing droplets on soap film[23]. In contrast to previous works, we describe here a spatial period-doubling instability which is rarely observed[24]. Nonlinear coupling between two commensurate modes also appears in post-buckling of cylindrical shells as reported in the classical work of Koiter (see ref. 25 and references therein).

The thin inextensible membrane of length L_0 is compressed horizontally by a distance $\Delta = L_0 - L$ along the x axis and is bound to an elastic foundation that initially fills the half-space $y < 0$. The system is assumed to remain invariant in the z direction (see Fig. 1). The projected length along the x axis, $L_0 - \Delta$, is given by

$$L_0 - \Delta = \int_0^{L_0} \mathrm{d}\ell \cos\phi \qquad (1)$$

where ℓ is the arc length measured along the curve. The quantity ϕ is the angle between the tangent to the surface and the horizontal. The derivative of this angle with respect to the arc length, $\partial_\ell \phi$, gives the local curvature of the membrane (partial derivatives $\partial/\partial\ell$ are written as ∂_ℓ). The relative compression ratio is given by $\delta = \Delta/L_0$.

The response of this thin membrane resting on an elastomer substrate is determined through minimization of the energy per unit of width, U. Two energetic contributions are to be considered: (1) the elastic bending energy of the thin sheet,

$$U_\mathrm{B} = \frac{B_\mathrm{m}}{2} \int_0^{L_0} \mathrm{d}\ell (\partial_\ell \phi)^2$$

where the parameter B_m is the bending stiffness of the membrane ($B_\mathrm{m} \simeq E_\mathrm{m} h^3$, E_m and h being its Young modulus and thickness); (2) the energy of deformation of the elastomer. The constraint of inextensibility of the membrane (1) is taken into account with the help of a Lagrangian multiplier F identified with the cross-sectional pressure per unit length. The Euler–Lagrange equation obtained from the energy of the system gives the equilibrium of normal forces along the membrane and is given by

$$B_\mathrm{m} \partial_\ell{}^4 y + F \partial_\ell{}^2 y + P_y = 0 \qquad (2)$$

where y and P_y are functions describing the vertical elevation of the membrane and the normal pressure from the elastomer acting on the membrane, respectively. At linear order, $P_y = KH(\partial_\ell y)$, where K is the stiffness coefficient of the foundation proportional

[1]Laboratoire Interfaces & Fluides Complexes, CIRMAP, Université de Mons — UMONS, 20 Place du Parc, B-7000 Mons, Belgium, [2]Laboratoire de Physique Statistique, Ecole Normale Supérieure, UPMC Paris 06, Université Paris Diderot, CNRS, 24 rue Lhomond, 75005 Paris, France.
*e-mail: pascal.damman@umons.ac.be.

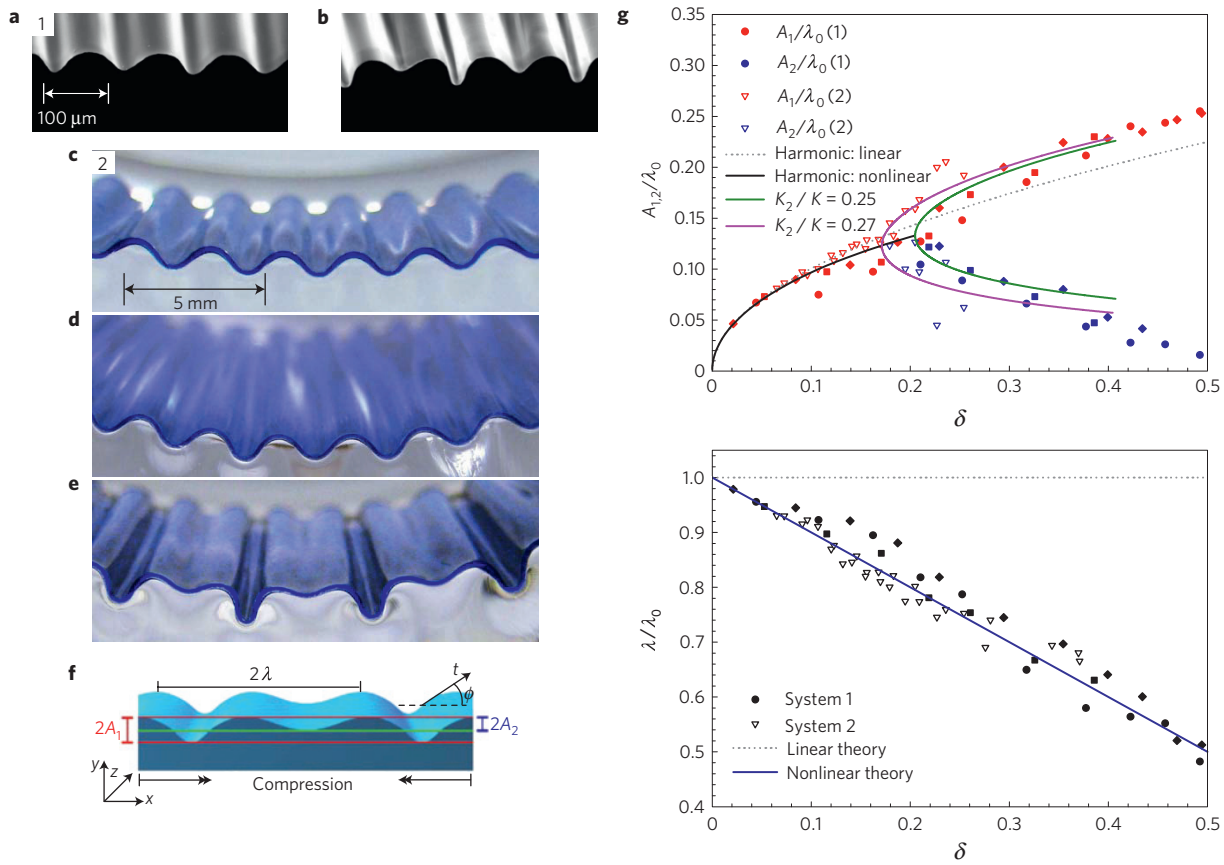

Figure 1 | Evolution of morphologies, wavelengths and amplitudes with compression. a,**b**, System 1. A PDMS foundation is cured with ultraviolet radiation–ozone, which modifies the elastic properties of its surface. The thickness of the membrane is about 10–20 μm depending on the irradiation time. The wavelength, λ_0, of the initial wrinkling instability is about 50–100 μm. **c**–**e**, System 2. A thin coloured stiff PDMS film is bound to a thick soft PDMS foundation. The thickness of the membrane is about 200 μm and the initial wrinkle wavelength is about 3 mm. The compression ratios, δ, are equal to 0.165, 0.19 and 0.24 for panels **c**, **d** and **e** respectively. **f**, The systems are compressed uniaxially along the x axis. The wavelength and amplitudes of the wrinkles are measured for successive values of the relative compression δ. **g**, Amplitudes (A_1, A_2) and wavelength, λ, as a function of the compression ratio δ. Experimental data for system 1 are reported with bullet, filled square and filled diamond symbols for 30 min, 1 h and 2 h of irradiation respectively whereas the open triangle is used for system 2. Results of the linear (dotted lines) and nonlinear (solid lines) theories are also reported. Before period doubling, the expression of the amplitude A computed from equations (1) is $A/\lambda_0 = \sqrt{\delta}/\pi(1-(3\delta/8)-(17\delta^2/128))$. The wavelength λ is computed from (7): $\lambda/\lambda_0 = 1-\delta+O(\delta^3,(B/\lambda_0)^2\delta^2)$, where B is the amplitude of the subharmonic mode.

to its Young modulus ($K = 2E(1-\sigma)/(1+\sigma)(3–4\sigma)$, where σ is the Poisson ratio) and H is the Hilbert transform. The first nonlinear contribution due to the elastomer can be computed for periodic deformation with one mode of wavenumber q and equation (2) then reduces to

$$B_m \partial_\ell{}^4 y + F\partial_\ell{}^2 y + Kqy + K_2 q^2 y^2 = 0 \qquad (3)$$

where K_2 is also proportional to the Young modulus ($K_2 = E(1–2\sigma)(13–16\sigma)/2(1+\sigma)(3–4\sigma)^2$; see Supplementary Information). The expression of the nonlinearity can also be deduced from a simple dimensional argument. From elasticity equations we expect a quadratic nonlinearity, and as there is no characteristic length-scale for the elastomer this term should be multiplied by the square of the wavenumber. Owing to the quadratic nonlinearity from the foundation, the equation (3) giving the profile of the membrane implies an up–down symmetry breaking: vertical extension and compression along the y axis are no longer equivalent. This equation can also be viewed as a spatial equivalent of a nonlinear oscillator, such as a simple pendulum, with which it shares many similarities.

Equation (3) reduces to a linear oscillator for small amplitudes of the instability. In this regime, the period is independent of the amplitude, in agreement with observation and usual theories. Indeed, nonlinear terms can be ignored for small amplitudes and the curvilinear and Cartesian coordinates coincide: $\ell \simeq x$, $\phi \simeq \partial_x y$. Equation (3) admits sinusoidal solutions $y(x) = A\cos(2\pi x/\lambda)$ provided that the pressure F and the wavelength of the wrinkling instability are related by

$$F(\lambda) = \frac{4\pi^2 B_m}{\lambda^2} + \frac{\lambda K}{2\pi}$$

This relation shows that below a threshold $F < F_c = 3q_0{}^2 B_m$ there is no associated wavelength and the membrane stays flat. At the threshold, $F = F_c$, the wrinkling instability emerges and a unique and constant wavelength, λ_0, is selected[3,26]

$$\lambda_0 = 2\pi\left(\frac{2B_m}{K}\right)^{\frac{1}{3}} \sim h\left(\frac{E}{K}\right)^{\frac{1}{3}}$$

The selection of this particular wavelength is obtained from a minimization of the energy through a minimization of F. The inextensibility constraint (1) gives the evolution of the amplitude of the instability as a function of the relative compression, $A = \pm\lambda_0\sqrt{\delta}/\pi$. However, neither the evolution of the wavelength with δ nor the period-doubling bifurcation are captured by this linear model.

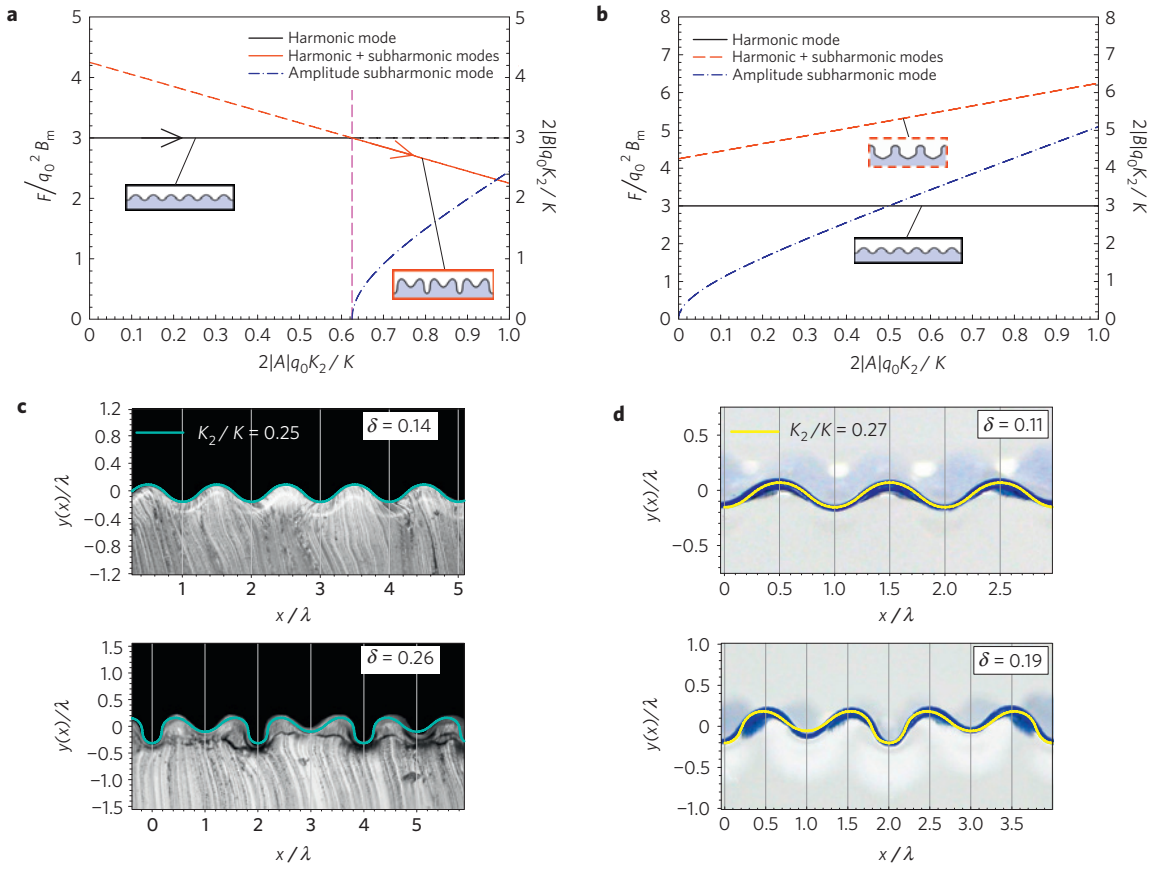

Figure 2 | Predictions of the model and comparison with experimental profiles. a,**b**, Evolution of the cross-sectional pressure F and of the amplitude B of the subharmonic mode as a function of the amplitude A of the harmonic mode. Arrows indicate the path followed by the systems during compression. Insets: Representative shapes of the membrane according to the value of F. **c**, Comparison between theoretical and experimental profiles of the membrane for system 1 for two values of δ. **d**, Comparison between theoretical and experimental profiles of the membrane for system 2 for two values of δ.

To determine the supercritical morphology, we study the stability of the single-wavelength pattern in the weakly nonlinear regime. We thus consider a small periodic perturbation, ϵu, characterized by a wavenumber k, of the nonlinear solution for the shape of the membrane: $y \to y + \epsilon u$, ϵ being arbitrarily small. The equation for the perturbation, u, in the leading order in the amplitude A of the instability is then given by

$$B_m \partial_\ell{}^4 u + F \partial_\ell{}^2 u + Ku = -2K_2 kAq_0 \cos(q_0 \ell) u \qquad (4)$$

The term appearing in the right-hand side of this equation is due to the quadratic nonlinearity of the foundation. Interestingly, this equation is similar to the Mathieu equation, describing resonance in parametric oscillators[27–30]. For usual forced oscillators, such as a simple pendulum with a variable length (the most famous example of this resonance is given by the giant censer, the Botafumeiro[29]), the unforced system is characterized by a given period and the extra wavenumber needed to produce a parametric resonance is provided by an external agent. For all amplitudes of the forcing, the resonance appears provided that forcing and oscillator wavenumbers are related through $k = q_0/2$.

In our system, however, we should also consider a constraint related to the minimization of F (that is, minimization of energy because $U(\delta) = L_0 \int_0^\delta F(\delta')\mathrm{d}\delta'$ where δ is the relative compression) determining the amplitude of the forcing term at which the 2λ mode emerges. Actually, the period-doubling instability cannot be observed for amplitudes smaller than a threshold (that is, a compression threshold, δ_2).

Equation (4) suggests that the profile should be described by a multimode solution of the form $y(\ell) = \sum_{k=1}^{\infty} C_k \cos(kq_0\ell/2)$, where C_k are the Fourier coefficients. The numerical analysis of equation (3), adapted to multimode periodic solutions, shows a very good agreement with experimental amplitudes $A_{1,2}$ (Fig. 1g). The relevance of the model is further demonstrated by the excellent agreement between experimental and calculated profiles (Fig. 2c,d). We should emphasize that the model relies on a single parameter, K_2/K, that determines the period-doubling threshold δ_2.

To preserve an explicit analysis and to capture the physics of the model, we restrict the following discussion to the ansatz $y(\ell) = A\cos(q_0\ell) + B\cos(q_0\ell/2)$. Substituting this ansatz in equation (3), we obtain a system of two equations in A, B and F, admitting two solutions. A trivial solution corresponds to the evolution before period-doubling: $F/(q_0{}^2B_m) = 3$ and $B = 0$ (A being determined by the inextensibility constraint). The second solution involving a subharmonic mode ($B \neq 0$) reads

$$\bar{F} = 17/4 + 2\bar{A} \qquad (5)$$

$$\bar{B}^2 = 2\bar{A}(5 + 8\bar{A}) \qquad (6)$$

where $\bar{F} = F/(q_0{}^2B_m)$, $\bar{A} = 2K_2Aq_0/K$ and $\bar{B} = 2K_2Bq_0/K$. Equation (5) is no longer invariant under a change of sign of A. Indeed, the amplitude A of the harmonic mode can be either positive or negative because the nonlinear system is characterized by an up–down symmetry breaking due to the quadratic nonlinearity of the foundation. Figure 2a,b shows the evolutions of both solutions with the amplitude, $\bar{A}$. The symmetry breaking

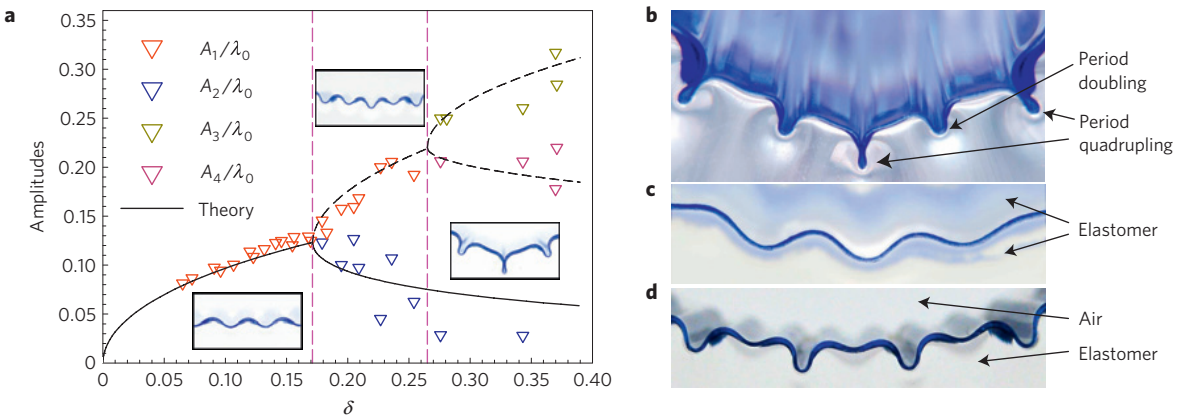

Figure 3 | Additional consequences of the up–down symmetry breaking for wrinkled patterns. a, Evolution of amplitudes for large compressions showing the period-quadrupling bifurcation in system 2. The solid curve is obtained numerically for $K_2/K = 0.27$. The dashed curve is added to help visualize the second bifurcation characterizing the period-quadrupling instability. **b**, Wrinkled structure showing the period-quadrupling instability ($\delta \simeq 0.37$). **c**, Profile of a thin stiff PDMS membrane resting in between two identical soft PDMS foundations for a relative compression $\delta \simeq 0.23$. **d**, Profile of a thin stiff PDMS membrane bound to a soft PDMS foundation for a relative compression $\delta \simeq 0.23$.

induces two regimes. For $\bar{A} > 0$, $\bar{F}$ is always larger than the value associated with the harmonic mode alone, that is, $\bar{F} = 3$. The corresponding shape for the membrane is forbidden and thus not observed experimentally; see Fig. 2b. In contrast, for $\bar{A} < 0$, the emergence of a subharmonic mode is energetically favourable ($\bar{F} < 3$) beyond a threshold value; see Fig. 2a. From equation (6), we observe that $\bar{B}$ starts to grow precisely from this threshold. This analysis does not, however, imply that a harmonic mode with a positive amplitude, $\bar{A} > 0$, is stable against subharmonic perturbations. Having found the energetically favourable pattern, we can use the translation invariance to generate equivalent patterns: $y(\ell - \pi/q_0) = -A\cos(q_0\ell) + B\sin(q_0\ell/2)$. The sign of A being now reversed implies that a harmonic mode with a positive amplitude is also unstable against subharmonic perturbations above the same threshold and leads to the same wrinkled pattern but translated.

The threshold for $\bar{A}$ implies the existence of a critical compression ratio, δ_2, for the onset of the period-doubling instability. Using the relation between A and δ at the lowest order, we obtain

$$\delta_2 = \left(\frac{5}{32(K_2/K)}\right)^2 \simeq 0.02\frac{(1-\sigma)^2}{(1-2\sigma)^2}$$

This critical compression ratio, δ_2, strongly decreases with the Poisson ratio of the elastic foundation. The values found numerically for the ratio $K_2/K \sim 0.25$ yield a Poisson ratio around 0.44, close to the value usually reported in the literature for PDMS (~0.48).

Moreover, this model should imply that, for larger amplitudes of the 2λ mode, a period-quadrupling bifurcation characterized by a wavelength 4λ would appear. This behaviour is indeed observed in Fig. 3a,b for compression ratios larger than 0.26. These observations clearly suggest that cascades of spatial period-doubling bifurcations can be observed for the elastic instability of a rigid membrane, provided that the up–down symmetry is broken. Such a cascade is known to lead to chaos after several bifurcations[15,16]. There is however a geometric limitation in our system: the evolution of the pattern saturates as soon as sharp folds appear (see Fig. 3b). Owing to finite thickness of the membrane, we experimentally reached at most period-quadrupling structures.

A further confirmation of our approach can be obtained. Our interpretation of the period-doubling bifurcation in a rigid membrane implies that the dynamics should be governed by nonlinear terms of even order, which break the up–down symmetry. Consequently, systems with up–down symmetry, such as a membrane on a liquid[8], do not develop a period-doubling instability. Interestingly, we could make trilayers restoring the symmetry. A system composed of an elastic membrane sandwiched in between two identical soft foundations does not exhibit the period-doubling bifurcation. Instead it develops patterns similar to those observed with floating membranes (Fig. 3b and c).

The second salient feature of the nonlinear wrinkling instability is the continuous decrease of the wavelength with the compression ratio δ. This effect arises from the change from curvilinear to Cartesian coordinates. The wavelength is measured along the horizontal x axis and the shape of the membrane is determined in curvilinear coordinates ℓ. For a periodic profile $y(\ell)$, with a wavelength λ_ℓ, $\lambda_x \equiv \lambda$ is given by

$$\lambda = \int_0^{\lambda_\ell} \mathrm{d}\ell \cos\phi = \int_0^{\lambda_\ell} \mathrm{d}\ell \sqrt{1-(\partial_\ell y)^2} \qquad (7)$$

The evolution of the wavelength along the horizontal x axis at the leading order in the amplitude is given by

$$\frac{\lambda}{\lambda_0} = 1 - \frac{(A\pi)^2}{{\lambda_0}^2} = 1 - \delta$$

in very good agreement with the experimental data in Fig. 1g.

The universal model describing the formation of wrinkled patterns on the basis of nonlinear oscillator dynamics should explain observations in very different fields. For example, a better understanding of the elastic instability of rigid membranes will help us to determine the exact mechanisms leading to the growth of wrinkled morphology in living systems. It is also a new blueprint to develop multiple-length-scale microfabrication techniques useful in the design of specific topography.

Methods

Experiments were carried out using PDMS elastomer (Sylgard 184) purchased from Dow Corning. Two different systems were studied. For system 1, a bare elastomer of PDMS is subjected to ultraviolet radiation in the presence of oxygen. Ozone is generated and will affect the crosslink density of the PDMS outer surface. The rigidity of the surface drastically increases with the irradiation time to finally yield a brittle overlayer covalently bound to the uncured elastomer. For system 2, multilayers were prepared by a simple assembly of monolayers of different elastic properties. The 'rigid' and 'soft' layers correspond to elastic modulus values of 1,200 and 10 kPa, respectively. To ensure a very strong adhesion between the two PDMS films and avoid delamination during the compression, these PDMS elastomers were assembled by contact after a plasma curing (in a Plasma Cleaner oven). The experimental set-up was a custom-built stretching–compressing device. The

ultraviolet/O_3-modified PDMS was compressed by using stretching–curing–release experiments. The measurements were achieved using image analysis from microtomed slices of the samples. The bilayer PDMS assembly was compressed by inducing a macroscopic radius of curvature. The measurements were made from macrophotography of the cross-sections of the samples (see Supplementary Information for further details).

Received 26 October 2009; accepted 26 August 2010; published online 31 October 2010

References

1. Witten, T. A. Stress focusing in elastic sheets. *Rev. Mod. Phys.* **79,** 643–675 (2007).
2. Bowden, N., Brittain, S., Evans, A. G., Hutchinson, J. W. & Whitesides, G. M. Spontaneous formation of ordered structures in thin films of metals supported on an elastomeric polymer. *Nature* **393,** 146–149 (1998).
3. Cerda, E. & Mahadevan, L. Geometry and physics of wrinkling. *Phys. Rev. Lett.* **90,** 074302 (2003).
4. Vandeparre, H. *et al.* Slippery or sticky boundary conditions: Control of wrinkling in metal-capped thin polymer films by selective adhesion to substrates. *Phys. Rev. Lett.* **99,** 188302 (2007).
5. Vandeparre, H. & Damman, P. Wrinkling of stimuloresponsive surfaces: Mechanical instability coupled to diffusion. *Phys. Rev. Lett.* **101,** 124301 (2008).
6. Huang, J. *et al.* Capillary wrinkling of floating thin polymer films. *Science* **317,** 650–653 (2007).
7. Jiang, H. *et al.* Finite deformation mechanics in buckled thin films on compliant supports. *Proc. Natl Acad. Sci.* **104,** 15607–15612 (2007).
8. Pocivavsek, L. *et al.* Stress and fold localization in thin elastic membranes. *Science* **320,** 912–916 (2008).
9. Diamant, H., Witten, T. A., Ege, C., Gopal, A. & Lee, K. Y. C. Topography and instability of monolayers near domain boundaries. *Phys. Rev. E* **63,** 061602 (2001).
10. Strupler, M. *et al.* Second harmonic microscopy to quantify renal interstitial brosis and arterial remodeling. *J. Biomed. Opt.* **13,** 054041 (2008).
11. Richman, D. P., Stewart, R. M., Hutchinson, J. W. & Caviness, V. S. Jr Mechanical model of brain convolutional development. *Science* **189,** 18–21 (1975).
12. Toro, R. & Burnod, Y. A morphogenetic model for the development of cortical convolutions. *Cereb. Cortex* **15,** 1900–1913 (2005).
13. Kücken, M. & Newell, A. C. A model for fingerprint formation. *Europhys. Lett.* **68,** 141–146 (2004).
14. Efimenko, K. *et al.* Nested self-similar wrinkling patterns in skins. *Nature Mater.* **4,** 293–297 (2005).
15. Feigenbaum, M. J. Quantitative universality for a class of nonlinear transformations. *J. Stat. Phys.* **19,** 25–52 (1978).
16. Feigenbaum, M. J. The universal metric properties of nonlinear transformations. *J. Stat. Phys.* **21,** 669–706 (1979).
17. Libchaber, A., Laroche, C. & Fauve, S. Period doubling cascade in mercury, a quantitative measurement. *J. Physique* **43,** L211–L216 (1982).
18. Guevara, M. R., Glass, L. & Shrier, A. Phase locking, period-doubling bifurcations, and irregular dynamics in periodically stimulated cardiac cells. *Science* **214,** 1350–1353 (1981).
19. Fox, J. J., Bodenschatz, E. & Gilmour, R. F. Period-doubling instability and memory in cardiac tissue. *Phys. Rev. Lett.* **89,** 138101 (2002).
20. Berger, C. M. *et al.* Period-doubling bifurcation to alternans in paced-cardiac tissue: Crossover from smooth to border-collision characteristics. *Phys. Rev. Lett.* **99,** 058101 (2007).
21. Melo, F., Umbanhowar, P. B. & Swinney, H. L. Hexagons, kinks, and disorder in oscillated granular layers. *Phys. Rev. Lett.* **75,** 3838–3841 (1995).
22. Venkataramani, S. C. & Ott, E. Spatiotemporal bifurcation phenomena with temporal period doubling: Patterns in vibrated sand. *Phys. Rev. Lett.* **80,** 3495–3498 (1998).
23. Gilet, T. & Bush, J. Chaotic bouncing of a droplet on a soap film. *Phys. Rev. Lett.* **102,** 014501 (2009).
24. Losert, W., Shi, B. Q. & Cummins, H. Z. Spatial period-doubling instability of dendritic arrays in directional solidification. *Phys. Rev. Lett.* **77,** 889–891 (1996).
25. Hutchinson, J. W. & Koiter, W. T. Postbuckling theory. *Appl. Mech. Rev.* **23,** 1353–1366 (1970).
26. Groenewold, J. Wrinkling of plates coupled with soft elastic media. *Physica A* **298,** 32–45 (2001).
27. McLachlan, N. W. *Theory and Application of Mathieu Functions* (Dover, 1962).
28. Blanch, G. Chapter 20: Mathieu Functions. in *Handbook of Mathematical Functions with Formulas, Graphs, and Mathematical Tables* (ed. Abramowitz, M.) (Dover, 1972).
29. Sanmartín, J. R. O Botafumeiro: Parametric pumping in the middle ages. *Am. J. Phys.* **52,** 937–945 (1984).
30. Van den Broeck, C. & Bena, I. in *Stochastic Processes in Physics, Chemistry, and Biology* 557 (eds Freund, J. A. & Pöschel, T.) 257–267 (Lect. Notes Phys., 2000).

Acknowledgements

The authors thank T. Witten, B. Davidovitch, H. Diamant, S. Desprez, C. Troetsler, S. Gabriele and G. Carbone for discussions. This work was supported by the Belgian National Funds for Scientific Research (Mandat Impulsion Scientifique), the Government of the Region of Wallonia (CORRONET and REMANOS Research Programmes) and the European Science Foundation (Eurocores FANAS programme, EBIOADI collaborative research project). F.B. acknowledges financial support from a return grant delivered by the Federal Scientific Politics.

Author contributions

F.B. and P.D. designed the experiments; F.B., H.V., A.S. and C.P. carried out the experiments; F.B., A.B. and P.D. developed the theoretical model; F.B. and P.D. wrote the manuscript.

Additional information

The authors declare no competing financial interests. Supplementary information accompanies this paper on www.nature.com/naturephysics. Reprints and permissions information is available online at http://npg.nature.com/reprintsandpermissions. Correspondence and requests for materials should be addressed to P.D.